Available online at www.sciencedirect.com
ScienceDirect
Earth and Planetary Science Letters 260 (2007) 277–296
EPSL
www.elsevier.com/locate/epsl

How surface complexes impact boron isotope fractionation: Evidence from Fe and Mn oxides sorption experiments

Emmanuel Lemarchand [a,*], Jacques Schott [a], Jérôme Gaillardet [b]

[a] LMTG-Université de Toulouse-CNRS-IRD-OMP, 14 Avenue Edouard Belin, 31400 Toulouse, France
[b] Laboratoire de Géochimie et Cosmochimie, Institut de Physique du Globe de Paris, Université Paris 7, UMR 7154, Tour 14/24 3ème étage, 4 place Jussieu, 75252 cedex 05, France

Received 22 December 2005; received in revised form 19 May 2007; accepted 20 May 2007
Available online 26 May 2007
Editor: C.P. Jaupart

Abstract

Although the pH-dependence of boron isotope fractionation between solution and precipitating minerals has been widely used in Earth Sciences, especially for reconstructing ancient seawater pH, the mechanisms by which boron adsorbs on solids or coprecipitates in minerals are still poorly known. Here we have investigated boron isotopic fractionation during its adsorption on goethite (α-FeOOH) and birnessite ($K_{0.1}MnO_{2.2}$,$0.9H_2O$) as a function of solution pH at T=25 °C and I=0.1 M. Maximum partition coefficients (Kd) between adsorbed and aqueous boron, equal to 39 and 34 for goethite and birnessite, respectively, are observed at pH=8–9. B adsorption at the surface of goethite induces its strong pH-dependent isotopic fractionation ranging from Δ=−40‰ (^{10}B enrichment on goethite) at pH<8, to zero at pH>10. During adsorption on birnessite at acid and neutral pH, boron isotopic fractionation is lower than during its sorption on goethite (Δ=−15‰), decreases (α increases) with increasing pH above pH=8, and reverses at pH>9: ^{11}B enrichment (+23‰ at pH=10.8) is observed at birnessite surface. Based on combined infrared (DRIFT) spectroscopic analysis and modeling of B speciation at oxides–solution interfaces, the observed isotopic fractionations can be rationalized by the formation of trigonal and tetrahedral boron inner-sphere complexes on goethite surface, and tetrahedral inner-sphere and trigonal outer-sphere and inner-sphere complexes on birnessite surface. B isotopic fractionation is strongly dependent on the structure of surface complexes formed: the high steric strain induced by the formation of trigonal boron bidendate binuclear complexes at goethite surface leads to a much higher isotopic fractionation (isotopically lighter sorbed boron) than that following the formation of tetrahedral bidendate binuclear complexes. Conversely, the formation at birnessite surface of trigonal complexes, having almost the same isotopic composition than aqueous boric acid, accounts for the heavier isotopic composition of birnessite than goethite boron, both at acid and alkaline pH.

These results show that, in nature, ^{11}B enrichment is expected in waters in equilibrium with iron or manganese oxides and that this enrichment is a function of pH that changes boron speciation in solution and at solid surfaces. This is typically the case for soil solution in Fe- and Mn-rich environments and in seawater. In addition, the markedly different isotopic fractionation factor, at the

* Corresponding author. Present address: Centre de Géochimie de la Surface, Ecole et Observatoire des Sciences de la Terre, 1 rue Blessig, 67087 Strasbourg Cedex, France. Tel.: +33 3 90 24 04 47; fax: +33 3 90 24 04 02.
E-mail addresses: Emmanuel.Lemarchand@illite.u-strasbg.fr (E. Lemarchand), schott@lmtg.obs-mip.fr (J. Schott), gaillard@ipgp.jussieu.fr (J. Gaillardet).

0012-821X/$ - see front matter
doi:10.1016/j.epsl.2007.05.039

same pH, of boron sorbed on goethite and birnessite (at pH=8.2, α is equal to 0.967 and 0.986 for goethite and birnessite, respectively) may be used to determine past ocean pH values without requiring knowledge of past isotopic composition.

Keywords: boron isotopes; surface speciation; iron oxides; manganese oxides; adsorption modeling; weathering proxy

1. Introduction

Variations in stable element isotopic abundances provide important constraints to understand the Earth's dynamics. Several rules have been established to explain stable isotope equilibrium abundance variations (O'Neil, 1986). Fractionation is larger for light elements and between isotopes with large relative mass differences. Moreover, the heavy isotopes tend to be enriched in phases where the element forms the strongest bonds. This is particularly the case when the element is in its high oxidation state or in its lowest coordination number (Schauble, 2004). Boron exhibits a single oxidation state in nature and, therefore, its isotopic fractionation is caused by changes in its coordination number or the ligands present in its coordination sphere. The two isotopes, ^{11}B and ^{10}B comprise 80 and 20% of the natural abundance of boron. Boron fractionation is generally expressed using the δ notation according to $\delta^{11}B = 1000 \times \frac{(({}^{11}B/{}^{10}B)_{sample} - ({}^{11}B/{}^{10}B)_{standard})}{({}^{11}B/{}^{10}B)_{standard}}$. Boron isotope abundances fluctuate widely at the surface of the Earth, from −50‰ for the most ^{11}B depleted materials to +59‰ in the most enriched (Barth, 1993). Boron exists in dilute solution as boric acid, a weak acid whose hydrolysis pKa is 9.23 at 25 °C (Baes and Mesmer, 1976). At typical Earth surface fluid pH, two forms of aqueous boron are present, the neutral trigonal boric acid ($B(OH)_3$) and the tetrahedral borate ion ($B(OH)_4^-$). Boron isotope fractionation occurs between the trigonal and tetrahedral configurations. For example, boron isotopes are fractionated by up to 30‰ between aqueous boric acid and tetrahedral borate ion; light boron is enriched in the borate ion (Klochko et al., 2006). In solids, boron generally exhibits tetrahedral coordination (Anovitz and Grew, 2002) and significant fractionation is thus expected when aqueous boric acid adsorbs on solid surfaces or coprecipitates.

A common application of boron isotopes in Earth Sciences is the determination of paleoocean pH and the paleoatmosphere CO_2 concentration. Partitioning between aqueous boric acid and the borate ion depends on solution pH. The boron isotopic composition of the bulk solution is not pH dependent, but the $\delta^{11}B$ of each of the B species is. As boron coprecipitates with carbonate minerals, the isotopic composition of boron provides a record of seawater pH if only one of the two aqueous species of boron (essentially borate ion) is incorporated into the solid lattice. This principle has been successfully applied to corals and forams by a number of authors (Hemming and Hanson, 1992; Sen et al., 1994; Hemming et al., 1995; Sanyal et al., 1996, 2000). Although the $\delta^{11}B$ of carbonates has been calibrated as a function of pH in living organisms, it appears that, in most cases, measured boron isotope compositions are not compatible with only incorporation of borate ions in the solids (Pagani et al., 2005). Authors have invoked vital effects to explain these observations (Hemming and Hanson, 1992; Hemming et al., 1995; Sanyal et al., 1996) but the exact mechanisms of boron incorporation are still unknown.

A second application of boron isotopes is related to chemical weathering. The interaction of boron with clays and humic acids has been demonstrated to significantly fractionate boron isotopes (Schwarcz et al., 1969; Palmer et al., 1987; Spivack et al., 1987; Lemarchand et al., 2005; Tossell, 2006). Lemarchand and Gaillardet (2006) showed that boron isotopes, because of surface exchange (Schwarcz et al., 1969; Keren and Mezuman, 1981; Keren et al., 1981; Keren and Gast, 1983; Goldberg and Glaubig, 1985; Goldberg and Glaubig, 1986a,b; Palmer et al., 1987; Spivack and Edmond, 1987; Goldberg and Glaubig, 1988; Gu and Lowe, 1990; Goldberg et al., 1993; Goldberg, 1999; Goldberg et al., 2000; Lemarchand et al., 2005; Tossell, 2006), can be used to couple hydrological and geochemical processes. In the Mackenzie River basin, boron isotope compositions are controlled by the hydrological conditions, shale weathering rates, and aqueous boron interactions with solid surfaces (Lemarchand and Gaillardet, 2006). These results indicate that the boron isotope composition of soil solutions, rivers, and groundwaters is probably dominated by adsorption and coprecipitation reactions.

Finally boron isotopes have proven to be efficient tracers of solid–fluid interactions in sedimentary basins (Williams et al., 2001a,b). Experiments have shown that boron isotopes are fractionated during diagenesis because of the massive incorporation of B (preferentially ^{10}B) into authigenic illites.

In the above processes, the boric acid dissociation constant and the boron fluid/solid partition coefficient are the two key parameters that control the observed isotope

composition variations. Since the pioneering studies of Schwarcz et al. (1969) and Spivack et al. (1987), however, the mechanisms controlling boron isotope fractionation during water–rock interactions have received little attention. In these papers, it was assumed that boron adsorption onto marine clay minerals occurs at equilibrium. Two fractionation coefficients between the solid and the solution were determined for boric acid and borate ion species but the type of complex formed and the exact reaction occurring between the solution and the solid were not determined.

This paper focuses on boron adsorption onto iron and manganese oxides. Although boron adsorption onto oxides has been extensively studied, in particular by the agronomical community (Sims and Bingham, 1968a,b; Goldberg and Glaubig, 1985; 1986b, 1988; Goldberg et al., 1993; Goldberg, 1999; Goldberg et al., 2000; de Bussetti et al., 1995; Goldberg, 1985, 2005), the related boron isotope fractionation is not known. In this study we performed boron adsorption experiments on well characterized goethite and birnessite surfaces as a function of solution pH, and measured the associated isotopic fractionation. Combining DRIFT (Diffuse Reflectance Infra-red Fourier Transform) spectroscopy of adsorbed boron and computer modeling, we characterized the structure of boron surface complexes and related boron isotope fractionation to the structure and thermodynamic properties of these complexes. We show that in addition to solution pH effects, the type of boron surface complex formed has a strong impact on isotopic fractionation.

2. Materials and methods

2.1. Materials

Pure synthetic goethite powder (Sikovit 10E172) was purchased from BASF (Germany). Characterization of this solid was carried out by Prelot et al. (2003a) using various techniques (X-ray diffraction, chemical analysis by ICPAES, TEM, high resolution SEM, adsorption isotherms). X-ray diffraction patterns are consistent with the orthorhombic structure of goethite (ASTM 29-713). Goethite chemical composition as derived from ICP-AES analysis is FeOOH,0.25 H2O and the main detected impurities are S, Si and Ca (2600, 720 and 650 ppm, respectively). The mean dimensions of goethite particles as deduced from SEM analyses are $600 \times 80 \times 80$ nm and their BET surface area (N_2 sorption) is 17.9 m^2/g. This value is in good agreement with BET specific surface area measured in this study (20 ± 1 m^2/g). Goethite powder used for pH-dependent sorption experiments and adsorption isotherms was washed ten times with MilliQ water (18.2 MΩ cm).

Birnessite was synthesized in this study according to Loganathan et al. (1977). 400 mL of 9 M HCl was added at 25 °C to 4 L of a well stirred 0.2 M $KMnO_4$ solution. Precipitated solid was separated by filtration, washed several times with milli-Q water and dried at 50 °C for 12 h. The crystallographic structure and chemical composition of synthesized Mn oxide was determined by X-ray diffraction (Inel G 3000 powder diffractometer), and thermo-gravimetric (Setaram MTB 10-8 microbalance) and wet chemistry analyses. The obtained XRD pattern is consistent with a poorly crystallized birnessite: signal/background ratio is low but narrow diffraction peaks can be observed at 1.41, 2.43, 3.67 and 7.25 Å, whereas several poorly defined peaks are apparent between 1.4 and 2.3 Å. H_2O content, as measured by thermo-gravimetric analysis, was 14.25 ± 1 wt.%. K and Mn concentrations are 41.8 ± 0.5 and 497 ± 5 mg/g, respectively. From these results, one can assume a composition $K_{0.1}MnO_{2.2}$, $0.9H_2O$. Birnessite powder specific surface area was 29 ± 1 m^2/g as measured by 3 points N_2 adsorption using the BET method.

Experimental solutions were prepared using doubly distilled HCl, and Prolabo Normapur H_3BO_3, NaCl and NaOH. Reagents were dissolved at the required concentrations with Milli-Q water. For NaOH, a supplementary purification step on the specific boron resin Amberlite IRA 743 was necessary to remove any trace of boron.

2.2. Adsorption experiments

2.2.1. pH dependent boron sorption experiments

Adsorption experiments were conducted at 25 ± 0.1 °C in acid-cleaned 30 mL polystyrene backbones. They consisted in adding a given amount of boric acid to a preequilibrated suspension of solid at pH ranging from 4 to 12. NaCl, HCl or NaOH were added to obtain a 0.1 M ionic strength and to maintain pH at the selected value. Typically, 0.2 mL of a 30 mM B ($B(OH)_3$) solution was added to 15 mL of a 0.2 M NaCl solution containing 0.6 g of goethite or birnessite; pH was adjusted at the desired value by adding boron free NaOH or bidistilled HCl and then solution volume was completed to 30 mL by adding Milli-Q water. Typical exposure time was about 2 weeks although preliminary kinetic experiments demonstrated that equilibrium was achieved in ~5 days. At the end of each run, pH was measured, the suspension was centrifuged 10 min at 2800 g, and the supernatant solution was filtrated through a 0.22 μm Nylon filter. The boron blank of the entire procedure described above never exceeded 120 ng, which represents 0.2% of the total amount of boron present in solution. Dissolved iron or manganese concentration, and

boron concentration and isotopic composition were measured in the filtrated solutions (see below).

2.2.2. Boron adsorption isotherms

Adsorption isotherm experiments were performed at 25±0.1 °C, pH 8.2±0.1 and I=0.1 M NaCl using 0.4 g/L of solid. 0.06 g of goethite or birnessite was introduced in a 180 mL polystyrene flask, and correct amounts of NaCl 0.1 M and B 2000 ppm-NaCl 0.1 M solutions (both adjusted at pH=8.2) were added to obtain boron aqueous concentrations ranging from 0.1 to 100 mM in a total volume of 150 mL. Exposure time was 7 days. During each run, pH was controlled and maintained constant by adding very small volumes of 0.01 or 0.1 M NaOH. At the end of the run, solid and solution were separated by centrifugation (10 mn, 2800 g), and the supernatant solution was filtrated at 0.22 μm. Sorbed boron was removed from goethite by adding three times 5 mL of NaOH 10^{-3} M on the solid during 2 days, and centrifuging the resulting suspension. For birnessite, the same procedure was used to remove sorbed boron, but HCl 10^{-3} M was used instead of NaOH. Boron concentration was measured in the filtrated and the supernatant solution. Measured desorbed B was corrected for aqueous boron remaining in interstitial solution.

2.3. Solution analysis

Solution pH was measured using a combination glass electrode (Schott Blue Line 12 pH) calibrated on the activity scale with NBS buffers (pH=4.01, 6.86 and 9.22 at 25 °C). Precision of pH measurements was ±1 mV (±0.02 pH unit). Aqueous boron concentrations were determined by the azomethin H colorimetric method (Capelle, 1961) at 420 nm using a Technicon analyzer II, with a 50 mm flow cell. Uncertainty on B analyses was $\pm 2\times10^{-6}$ M with a detection limit of 4.5×10^{-6} M. Fe and Mn concentrations in solution were determined by flameless atomic absorption (Perkin Elmer 5100 PC) with an uncertainty of ±1% and a detection limit of 9×10^{-8} M.

2.4. Determination of boron isotopic ratio

Only solute boron isotopic ratios were measured. The mass conservation equation allowed to approximate adsorbed B isotopic composition from its aqueous composition:

$$R_{\mathrm{Bads}} = \frac{m_{\mathrm{Btot}} \cdot R_{\mathrm{Btot}} - m_{\mathrm{Bsol}} \cdot R_{\mathrm{Bsol}}}{m_{\mathrm{Bads}}} \quad (1)$$

where m_{Bads}, m_{Bsol}, m_{Btot}, R_{Bads}, R_{Bsol} and R_{Btot} stand for the mass and isotopic composition of adsorbed, aqueous and total boron, respectively.

Analyses of B isotopes were performed on two different mass spectrometers. Samples from sorption experiments on goethite were analyzed with a Thomson THN 206 (30 cm radius, 60°) at the Institut de Physique du Globe, Paris. Samples from experiments on birnessite were analyzed with a Thermo Finighan MAT 262 (23° cm radius, 90°) at the Laboratoire des Mécanismes et Tranferts en Géologie, Toulouse. The accelerating voltage was fixed at 6 and 8 kV for analyses on Thomson THN 2006 and Thermo Finighan MAT 262, respectively. For the two sets of analyses, ion beams were collected in a single collector cup coupled to a 10^{11} Ω resistor. The isotopic ratios were determined using an optimized version of PTIMS (positive thermal ionization mass spectrometry) cesium borate technique ($Cs_2BO_2^+$) (Spivack and Edmond, 1986), with addition of graphite, mannitol and HCl. Fe or Mn was removed from the solution using the cationic resin Bio-Rad AG 50W-X8. Then, the procedure for B chemical purification consists in successive loading, rinsing and elution on the boron specific resin Amberlite IRA 743. We used successively a 10 μL and a 3 μL resin column. The final volume of purified solution is equal to 40 μL. Boron is then separated from traces of organic matter originating from the resin column using the "microsublimation" technique (Gaillardet et al., 2001; Lemarchand et al., 2006). The purified boric acid is evaporated at 60 °C and dissolved in 2 μL HCl 0.1 M, 1 μL mannitol 0.055 M and 1 μL CsOH 0.031 M. The obtained solution is loaded step by step on a tungsten filament previously coated with 1 μL of a 13 g/L graphite solution, and dried under heating lamp for 15 min. This filament is introduced in the mass spectrometer, and boron isotopic ratios are determined by successive analysis of the ion current at mass 308 ($^{133}Cs_2^{10}B^{16}O_2$), 309 ($^{133}Cs_2^{11}B^{16}O_2$), and 306.5 (reference mass). A typical analysis consists in 15 blocs of 10 cycles. The external reproducibility for analysis of standard NIST SRM 951 is 0.38‰ (±2σ). The ^{17}O contribution is corrected by deducing 0.00078 to the measured 309/308 mass ratio. Repeated analyses of the standard gave an averaged isotopic ratio of 4.05123±0.00025 and 4.05074±0.00045 with the Thomson THN 206 and the Thermo Finnigan MAT 262, respectively. The boron blank of this chemical procedure, as measured by isotopic dilution, is 1.4 ng, which represents less than 0.6% of the total amount of B analyzed. Reproducibility between sample replicate analyses was better than 0.4‰.

2.5. Diffuse-Reflectance Infrared Fourier-Transformed (DRIFT) spectroscopy

Boron complexes formed at pH=7.3 and pH=9.2 on the surface of birnessite and at pH=7.1 and pH=9.8 on the surface of goethite were characterized by DRIFT spectroscopy. Samples were prepared by equilibrating a solid suspension (goethite: 30 g/L, birnessite: 10 g/L) with 0.1 mol/L boric acid at the required pH. After separation from the solution *via* centrifugation at 2800 g, the solid phase was dried for 12 h at 40 °C.

The DRIFT (Diffuse Reflectance Infra-red Fourier Transform) spectra were recorded on a Bruker IFS88 FTIR spectrometer with an MCT detector by means of a diffuse reflectance attachment. All the accessories were from Harrick Scientific Co. The spectrometer was purged with CO_2-free dry air (Balston Filter). 50 mg of dry powder were dispersed in 350 mg of KBr, and lightly packed into a 5 mm diameter microsampling cup. The spectra were taken at 4 cm^{-1} resolution by co-adding up to 200 scans in the 4000–500 cm^{-1} region. The unit of intensity was defined as $\log(R/R_0)$ where R_0 and R are the reflectivities of the system with and without the investigated sample, respectively. The contribution of atmospheric water was subtracted from the spectra.

2.6. Modeling

2.6.1. Speciation calculations

The standard state adopted in the present study for both aqueous and surface species is unit activity for a hypothetical, one molal ideal solution. The activity coefficients γ_i of charged aqueous species were calculated using the Davies equation:

$$\log\gamma_i = Az_i^2 \cdot \left(\frac{\sqrt{I}}{1+\sqrt{I}} - C \cdot I\right) \quad (2)$$

where A and C are semi-empirical parameters that depend on temperature and the relative permittivity of the solvent. For this study performed in aqueous solution at 25 °C, A and C values were set to 0.509 and 0.3, respectively. I represents the ionic strength of solution, and z_i denotes the charge of the ith species. The thermodynamic constants for boric acid dissociation were taken from (Baes and Mesmer, 1976) and that for the formation of the $NaB(OH)_4^0$ ion pair was from (Pokrovski et al., 1995).

Formation constants and distribution of boron surface complexes were calculated from pH-dependent adsorption experiments using FITEQL 3.2 software (Herbelin and Westall, 1996). Three different 2-pK surface complexation models were tested: the constant capacitance model, the diffuse layer model, and the triple layer model. For each oxide, we considered a single type of surface hydroxyl group (SOH) that can undergo protonation or deprotonation reactions, and can coordinate aqueous species including boric acid. Aqueous and surface reactions involved in these calculations are listed in Appendix A.

2.6.2. Isotopic calculations

The boron isotope fractionation factor, α, between solution and goethite or birnessite surface was deduced from boron aqueous and surface speciation calculations. Isotope fractionation factors $\alpha_{Boxy\text{-}III}=(^{11}B/^{10}B)_{Boxy}/(^{11}B/^{10}B)_{III}$ are defined between aqueous boric acid ($B(OH)_3^0$) and boron surface species (B_{oxy}). With this convention, the fractionation factor measured at equilibrium between the solution and adsorbed boron can be deduced from the following equation:

$$\alpha_{oxy-solution} = \frac{\sum([B_{oxy}]\cdot\alpha_{Boxy-III})}{\sum[B_{oxy}]} \times \frac{[B(OH)_3]+[B(OH)_4^-]+[NaB(OH)_4]}{[B(OH)_3]+([B(OH)_4^-]+[NaB(OH)_4])\alpha_{IV-III}} \quad (3)$$

where $\alpha_{IV-III}=(^{11}B/^{10}B)_{IV}/(^{11}B/^{10}B)_{III}$ is the isotopic fractionation factor between borate ion, boric acid and $[B_{oxy}]$ stands for the concentration of a given surface complex and all the other $[i]$ represent the concentration of boron aqueous species. Least square fitting of Eq. (3) was used to extract values of $\alpha_{Boxy\text{-}III}$ from experimentally measured α and the calculated distribution of boron aqueous and surface species.

3. Results

3.1. Adsorption results

3.1.1. pH dependent adsorption

Results of boron sorption on goethite and birnessite at 25 °C and 0.1 M are listed in Table 1, and the partition coefficient Kd between adsorbed and aqueous boron ($Kd=(m_{Bads}/m_{solid})/(m_{Baq}/m_{solution})$) is plotted as a function of solution pH in Fig. 1. In agreement with previous results for iron oxides (Sims and Bingham, 1968a; Goldberg and Glaubig, 1985; Goldberg, 1985; Su and Suarez, 1995), humic acids (Gu and Lowe, 1990; Goldberg, 2005; Lemarchand et al., 2005) and clay minerals (Keren et al., 1981; Keren and Mezuman, 1981; Keren and Gast, 1983; Goldberg and Glaubig,

Table 1
Initial conditions and final results of adsorption and isotopic experiments onto goethite and birnessite

Experiment	1	2	3	4	5	6	7	8	9	10	11	12	13	14	15	16	17
Goethite																	
Final pH	4.99± 0.01	5.79± 0.01	6.33± 0.01	6.88± 0.01	7.05± 0.01	7.18± 0.01	7.38± 0.01	7.83± 0.01	7.86± 0.01	8.18± 0.01	8.67± 0.01	9.02± 0.01	9.14± 0.01	9.75± 0.01	10.28± 0.01	10.60± 0.01	10.95± 0.01
Goethite (g/L)	15.4± 0.039	15.7± 0.039	15.6± 0.039	14.0± 0.035	19.9± 0.050	15.8± 0.039	22.5± 0.056	25.8± 0.065	14.4± 0.036	25.3± 0.063	26.1± 0.065	14.6± 0.037	25.6± 0.064	21.3± 0.053	21.5± 0.054	14.6± 0.036	21.0± 0.053
Total B (ppm)	2.100± 0.021	2.135± 0.021	2.151± 0.022	1.989± 0.020	2.245± 0.022	2.093± 0.021	2.212± 0.022	2.187± 0.022	2.069± 0.021	2.029± 0.020	2.095± 0.021	2.063± 0.021	2.066± 0.021	2.078± 0.021	2.026± 0.020	2.030± 0.020	2.062± 0.021
NaCl (mol/L)	0.1	0.1	0.1	0.1	0.1	0.1	0.1	0.1	0.1	0.1	0.1	0.1	0.1	0.1	0.1	0.1	0.1
Final dissolved B (ppm)	1.794± 0.018	1.673± 0.017	1.555± 0.016	1.383± 0.014	1.381± 0.014	1.404± 0.014	1.218± 0.012	1.114± 0.011	1.363± 0.014	1.016± 0.010	1.049± 0.010	1.350± 0.014	1.081± 0.011	1.388± 0.014	1.655± 0.017	1.852± 0.019	1.844± 0.018
% adsorbed B	15±1.2	22±1.1	28±1.0	30±1.0	38±0.9	33±0.9	45±0.8	49±0.7	34±0.9	50±0.7	50±0.7	35±0.9	48±0.7	33±0.9	18±1.2	9±1.3	11±1.3
Kd	11±1.1	18±1.2	25±1.3	31±1.5	31±1.2	31±1.3	36±1.1	37±1.1	36±1.5	39±1.1	38±1.1	36±1.5	36±1.1	23±1.0	10±0.8	7±1.1	6±0.8
$^{11}B/^{10}B$ in solution	4.02648± 0.00161	4.03677± 0.00161	4.04659± 0.00162	4.04870± 0.00162		4.05260± 0.00162	4.07458± 0.00163		4.04736± 0.00162	4.06707± 0.00163		4.03538± 0.00161	4.04530± 0.00162	4.02047± 0.00161		4.00311± 0.00160	4.00281± 0.00160
$^{11}B/^{10}B$ in goethite	3.84986± 0.01949	3.87005± 0.01300	3.88112± 0.01040	3.89119± 0.00992		3.89488± 0.00875	3.91015± 0.00589		3.91077± 0.00824	3.93411± 0.00471		3.93508± 0.00704	3.95176± 0.00436	3.96100± 0.00609		3.97577± 0.02497	3.98312± 0.02031
α	0.9561± 0.0049	0.9587± 0.0032	0.9591± 0.0026	0.9611± 0.0025		0.9611± 0.0022	0.9596± 0.0015		0.9663± 0.0021	0.9673± 0.0012		0.9751± 0.0018	0.9769± 0.0011	0.9852± 0.0016		0.9932± 0.0063	0.9951± 0.0051

Experiment	1	2	3	4	5	6	7	8	9	10	11	12	13	14	15	16	17	18
Birnessite																		
Final pH	4.99± 0.01	5.53± 0.01	5.95± 0.01	6.44± 0.01	6.62± 0.01	6.95± 0.01	7.31± 0.01	7.48± 0.01	7.80± 0.01	8.21± 0.01	8.28± 0.01	8.79± 0.01	9.25± 0.01	9.32± 0.01	9.81± 0.01	10.31± 0.01	10.33± 0.01	10.76± 0.01
Manganese oxyde (g/L)	18.9± 0.047	19.2± 0.048	19.1± 0.048	19.4± 0.049	18.9± 0.047	19.4± 0.048	19.5± 0.049	19.4± 0.048	19.1± 0.048	19.7± 0.049	19.1± 0.050	19.8± 0.047	19.5± 0.049	18.9± 0.047	18.9± 0.049	19.6± 0.047	17.9± 0.045	18.9± 0.048
Total B (ppm)	1.924± 0.019	1.963± 0.020	1.895± 0.019	1.933± 0.019	1.943± 0.019	1.928± 0.019	1.961± 0.020	1.972± 0.020	1.992± 0.020	2.004± 0.020	1.949± 0.019	1.951± 0.020	1.912± 0.019	1.954± 0.020	1.920± 0.019	1.949± 0.019	1.832± 0.018	1.906± 0.019
NaCl (mol/L)	0.1	0.1	0.1	0.1	0.1	0.1	0.1	0.1	0.1	0.1	0.1	0.1	0.1	0.1	0.1	0.1	0.1	0.1
Final dissolved B (ppm)	1.815± 0.018	1.531± 0.015	1.525± 0.015	1.394± 0.014	1.439± 0.014	1.383± 0.014	1.321± 0.013	1.322± 0.013	1.297± 0.013	1.240± 0.012	1.210± 0.012	1.161± 0.012	1.257± 0.013	1.365± 0.014	1.476± 0.015	1.704± 0.017	1.586± 0.016	1.778± 0.018
% adsorbed boron	6±1.3	22±1.1	19±1.1	28±1.0	26±1.0	28±1.0	33±1.0	33±0.9	35±0.9	38±0.9	38±0.9	40±0.8	34±0.9	30±1.0	23±1.1	13±1.2	13±1.2	7±1.3
Kd	3±0.8	15±0.9	13±0.9	20±1.0	19±1.0	20±1.0	25±1.1	25±1.1	28±1.1	31±1.2	32±1.3	34±1.2	27±1.1	23±1.0	16±0.9	7±0.8	9±0.9	4±0.8
$^{11}B/^{10}B$ in solution			4.01804± 0.00161	4.01856± 0.00161				4.01630± 0.00161	4.02709± 0.00161		4.02666± 0.00161	4.01810± 0.00161	3.99939± 0.00160	4.00827± 0.00160	3.99901± 0.00160			3.99913± 0.00160
$^{11}B/^{10}B$ in birnessite			3.95378± 0.01139	3.95466± 0.00747				3.96908± 0.00607	3.96529± 0.00603		3.97088± 0.00549	3.98701± 0.00480	4.00327± 0.00559	3.99912± 0.00653	4.02713± 0.00873			4.09432± 0.03276
α			0.9840± 0.0029	0.9841± 0.0019				0.9882± 0.0016	0.9847± 0.0015		0.9861± 0.0014	0.9923± 0.0013	1.0010± 0.0015	0.9977± 0.0017	1.0070± 0.0022			1.0238± 0.0082

$Kd=(m_{Badsorbed}/m_{solid})/(m_{Baq}/m_{solution})$ is the partition coefficient and $\alpha=(^{11}B/^{10}B)_{ads}/(^{11}B/^{10}B)_{sol}$ is the boron isotopes fractionation factor. Initial $^{11}B/^{10}B$ ratio in solution is equal to 4.00072.

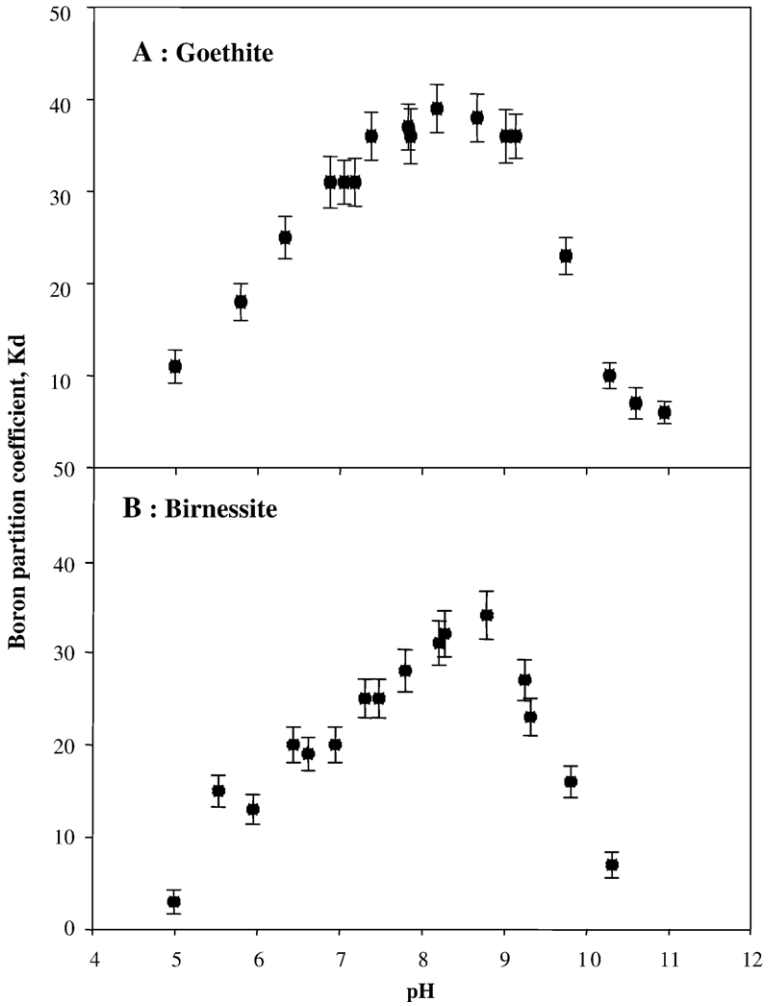

Fig. 1. Boron adsorption on goethite (A) and birnessite (B): boron partition coefficient Kd (Kd=($m_{Badsorbed}/m_{solid}$)/($m_{Baq}/m_{solution}$)) between adsorbed and aqueous boron as a function of pH at 25 °C and I=0.1 M. Error bars were calculated taking account of concentration measurement uncertainties of 1%.

1986a), the boron adsorption envelop for both goethite and birnessite is bell-shaped like typical oxyanions sorption curves. Boron sorption increases with pH up to pH 8.5–9, and decreases with further pH increase because of the repulsion between borate ion and negatively charged surface sites. The maximum value of Kd is slightly higher for goethite (40) than for birnessite (35). Kd values obtained in this study compare well with those deduced from Goldberg and Glaubig (Goldberg and Glaubig, 1985) sorption experiments at 25 °C on goethite (Kd=11), hematite (Kd=6.4) and amorphous iron oxide (Kd=170).

3.1.2. Adsorption isotherms

Boron adsorption isotherms on goethite and birnessite at pH=8.2 are presented in Fig. 2 where sorbed boron concentration (mmol/$kg_{metal\ oxyde}$) is plotted as function of its aqueous concentration (mmol/L) at equilibrium. Both isotherms can be modeled within the framework of a two term series Langmuir equation (Stumm and Morgan, 1996):

$$\Gamma_B = \frac{\Gamma_1 K_1 [B]}{1 + K_1 [B]} + \frac{\Gamma_2 K_2 [B]}{1 + K_2 [B]} \quad (4)$$

where K_1 and K_2 are equilibrium constants, Γ_B, Γ_1 and Γ_2 represent total B surface concentration and maximum B surface concentration for hypothetical reactions 1 and 2, respectively, and [B] is boron aqueous concentration at equilibrium. Description of boron sorption by Eq. (4) likely indicates that either two different surface species contribute to boron sorption or a single boron species is

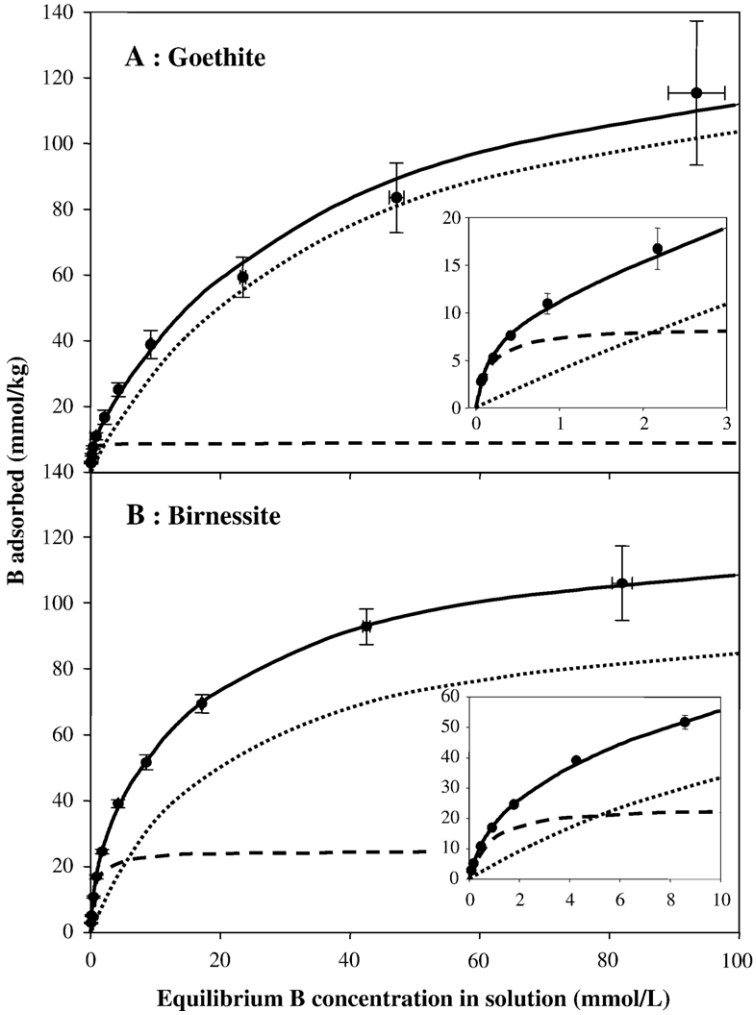

Fig. 2. Concentration of boron sorbed at the surface of goethite (A) and birnessite (B) as a function of aqueous boron concentration (Langmurian adsorption isotherm) at pH=8.2, I=0.1 M, and T=25 °C. The symbols represent the experimental data (errors bars take account of an uncertainty of 1% on boron chemical analyses). The dashed and dotted lines represent the Langmuir equation fit of two hypothetical complexes, the solid line is the sum of dashed and dotted line. Values of fit parameters are K_1=0.58, K_2=0.0025, Γ_1=8.5 mmol/kg, Γ_2=141.7 mmol/kg for goethite, and K_1=0.12, K_2=0.0045, Γ_1=23.8 mmol/kg, Γ_2=102.7 mmol/kg for birnessite.

sorbed on two sites with different affinities. The maximum boron sorption capacities calculated from equation 14 are equal to 4.53 B/nm^2 and 2.54 B/nm^2 for goethite and birnessite, respectively.

3.2. DRIFT spectroscopy

DRIFT spectra (800 to 1500 cm^{-1}) of pure goethite and boric acid adsorbed on goethite at pH 7.1 and 9.8, and I=0.1 M are shown in Fig. 3-A, whereas DRIFT spectra of pure birnessite and boron adsorbed on birnessite at pH 7.2 and 9.2, and I=0.1 M are shown in Fig. 3-B. It can be seen that boron sorption is characterized by several absorption bands between 900 and 1500 cm^{-1}, in agreement with results of Su and Suarez (1995) and Peak et al. (2003). Assignment of B sorption bands can be carried out based on the results of Peak et al. who performed a detailed ATR–FITR spectroscopic study of boric acid sorbed on hydrous ferric oxide. The four main regions of boron infrared absorbance determined by Peak et al. are identified on Fig. 3 by vertical gray bands numbered from 1 to 4. The peak around 1400 cm^{-1} (1) is assigned to the asymmetric stretching band of boric acid or trigonal outer-sphere boron complexes and the peaks between 1200 and 1350 cm^{-1} (2) to the asymmetric stretching bands of trigonal inner-sphere boron. B–O–H bending is characterized by a band around 1150 cm^{-1} (3) for both trigonal and tetrahedral

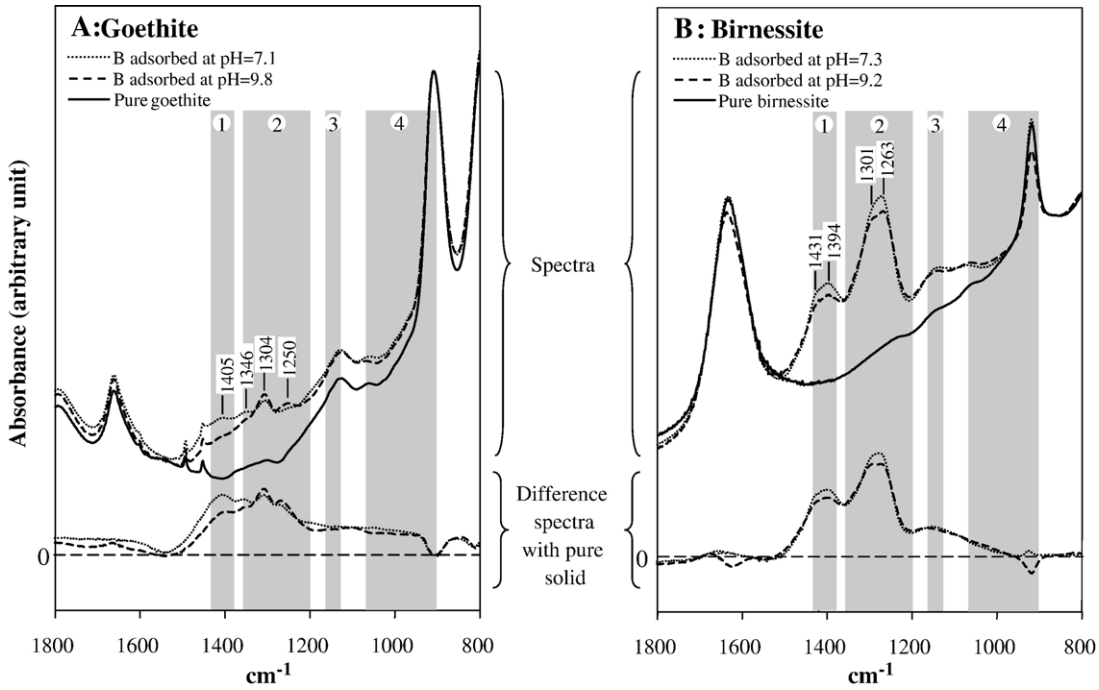

Fig. 3. DRIFT spectra of boron adsorbed at 25 °C and I=0.1 M on goethite (A) and birnessite (B). Initial aqueous boron concentration is 0.1 mol/L in suspensions containing 30 and 10 g/L of goethite and birnessite, respectively.

boron whereas the peaks occurring between 900 and 1050 cm^{-1} (4) are assigned to the asymmetric stretching band of tetrahedral boron and the symmetric stretching band of trigonal inner-sphere boron. On both goethite and birnessite, the presence of trigonal inner-sphere boron complexes is clearly identified by peaks between 1200 and 1350 cm^{-1}. The peaks observed at 1405 cm^{-1} on goethite and at 1394 and 1431 cm^{-1} on birnessite likely correspond either to a boron outer-sphere trigonal complex or to aqueous boric acid present in interstitial solution. The strong decrease of this peak intensity between pH 7.1 and 9.8 on goethite strongly suggests the presence of aqueous boric acid, whereas the presence of two peaks on birnessite probably correspond to the presence of both aqueous boric acid and boron trigonal outer-sphere complexes. The formation of tetrahedral boron surface complexes could not be detected because of the presence of a strong absorption peak centered at 908 and 918 cm^{-1} for goethite and birnessite, respectively, that corresponds to metal-hydroxides vibration bands (Abou-El-Sherbini, 2002; Ruan et al., 2002). However, the intensity of the ~930 cm^{-1} band is enhanced for goethite samples subjected to boron sorption. In accordance with Su and Suarez (1995) and Peak et al. (2003) peak assignments, this likely indicates that tetrahedral boron is present at the surface of goethite.

In summary, our DRIFT study clearly shows the presence of an inner-sphere trigonal complex at goethite surface, and of both inner-sphere and outer-sphere trigonal complexes at birnessite surface. The probable formation of tetrahedral boron surface complexes is hidden by metal-hydroxide IR bands.

3.3. Isotopic fractionation

3.3.1. Goethite

Results listed in Table 1 provide, for each pH, $^{11}B/^{10}B$ ratios in solution and at goethite surface, and boron isotopic fractionation factor between goethite surface and aqueous solution:

$$\alpha_{oxy-solution} = \frac{(^{11}B/^{10}B)_{adsorbed}}{(^{11}B/^{10}B)_{solution}}. \quad (5)$$

The variation of α as a function of solution pH is illustrated in Fig. 4-A. It can be seen that it is consistent with a sigmoidal dependence of α on pH. A roughly constant, very strong isotopic fractionation ($\alpha_{oxy\text{-}solution}$=0.958, Δ~−44‰) occurs at pH≤7.5, with ^{10}B enrichment on the goethite surface. At higher pH, isotopic fractionation decreases slowly and approaches zero ($\alpha_{oxy\text{-}solution}$~1) at pH=11. Boron isotopic fractionation measured at

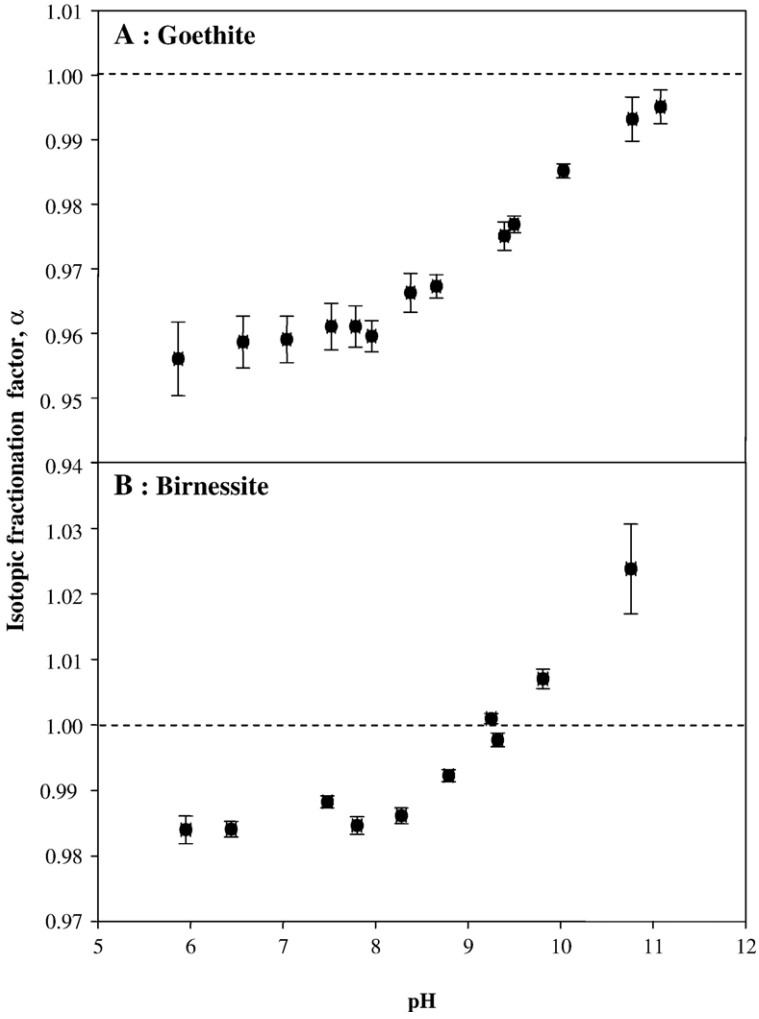

Fig. 4. Boron isotopic fractionation following its adsorption at 25 °C and I=0.1 M onto goethite (A) and birnessite (B): variation of boron isotopes fractionation factor as a function of solution pH. Error bars account for analytical uncertainty of 1% and 0.4 ‰ on boron concentration and isotopic measurements, respectively.

slightly acidic and circum neutral pHs is significantly higher than that following boron sorption on marine clays ($\alpha_{oxy\text{-}solution}$=0.968; Palmer et al., 1987) and humic acids ($\alpha_{oxy\text{-}solution}$=0.975; Lemarchand et al., 2005) or its incorporation in carbonate minerals ($\alpha_{oxy\text{-}solution}$=0.977–0.981; Hemming et al., 1995; Sanyal et al., 1996; Sanyal et al., 2000).

3.3.2. Birnessite

Results are listed in Table 1 and illustrated in Fig. 4-B where boron isotopic fractionation factor between birnessite surface and aqueous solution is plotted as a function of pH. As for goethite, birnessite surface is enriched in ^{10}B at acidic and circum neutral pH but isotopic fractionation is much lower ($\alpha_{oxy\text{-}solution}$ ~ 0.985, Δ ~ −15‰). At pH>8, isotopic fractionation decreases with pH, equals zero ($\alpha_{oxy\text{-}solution}$=1) at pH ~ 9, and reverses ($\alpha_{oxy\text{-}solution}$>1) at pH>9.5 with surface enrichment in ^{11}B. At pH=10.76, $\alpha_{oxy\text{-}solution}$=1.023 ($\Delta$=+23‰). It is worth noting that total Δ variation between acidic and alkaline conditions (5<pH<11) approaches 40‰ which is close to that observed for the similar pH range at goethite surface (42‰).

4. Modeling

The aim of modeling was to calculate the distribution and isotopic composition of the different boron surface complexes formed in order to decipher the impact of complexes structural parameters on isotopic fractionation. The formation constants and distributions of boron surface complexes identified by DRIFT spectroscopy

were deduced from experimental adsorption curves using FITEQL software. Then, from the calculated distributions of aqueous and surface boron complexes, the isotopic composition of each complex was calculated to fit the experimental isotopic fractionation curves.

4.1. Adsorption modeling

4.1.1. Goethite

Based both on our DRIFT study that did not provide evidence for the formation of B outer-sphere complexes and the recent results of Goldberg (2005) that showed very weak dependence on ionic strength of B sorption at goethite surface, adsorption modeling was performed assuming that boron only formed inner-sphere surface complexes. Boron sorption was quantified within the framework of the constant capacitance (CCM) and the diffuse layer (DLM) models, assuming, in agreement with previous and the present IR studies, the formation of both trigonal and tetrahedral complexes. In both models, surface site concentration was set equal to the value derived from our isotherm experiment (4.53 site/nm^2) whereas the specific surface area, as measured by N_2 absorption using the BET method, was set equal to 20 m^2/g. In a first step, values for goethite surface protonation constants were taken from Sverjensky (Sverjensky, 2005), and values for boron surface complexation constants were calculated using FITEQL 3.2 software (Herbelin and Westall, 1996). A second model calculation was performed in which goethite surface protonation constants and boron surface complexation constants were simultaneously fitted. Both the diffuse layer and the constant capacitance model provided comparable adsorption curves and surface constants but, in the case of the constant capacitance model, a correct fit of experimental data was obtained only for a value of the capacitance of the electric double layer ($C \geq 2$ F/m^2) significantly higher than that commonly adopted for sorption studies on goethite (1.2 F/m^2) (Goldberg, 1985; Goldberg, 1999; Sverjensky, 2005). For this reason, we present only the results obtained with the diffuse layer model. Model parameters values are listed in Table 2, and boron surface speciation as a function of pH is illustrated in Fig. 5-A and B. In Table 2 the goodness of fit expressed by WSOS/DF (the weighted sum of squares of the difference between experimental and fitted values divided by the degree of freedom) is also provided. In principle, the best fit is obtained for the lowest value of WSOS/DF.

Fig. 5-A shows that boron sorption modeled by fitting only boron sorption constants are not in accord with experimental data, particularly at pH<7. The best description of experimental data is obtained with goethite protonation/deprotonation pKa values of 7.5 and 11.2. This model accurately describes the overall experimental boron adsorption as a function of pH with the presence of two inner-sphere boron complexes, a neutral trigonal complex at pH<10, and a negative tetrahedral complex that becomes predominant at pH≥9 (Fig. 5-B).

Table 2
Modeling of boron adsorption at the surface of goethite and birnessite at 25 °C

	Goethite (diffuse layer model)		Birnessite (triple layer model)	
	Only B sorption constants optimized	Every constants optimised	Only B sorption constants optimized	Every constants optimised
pKa_1	6.4 [a]	7.5	2.3 [b]	7.25
pKa_2	12.0 [a]	11.2	4.2 [b]	10.43
$\log K^{+}_{Na}$			−3.3 [b]	−9.53
$\log K_{Bin}$	2.4	2.3	0.9	1.75
$\log K_{B-in}$	−6.6	−6.6	−1.2	−6.56
$\log K_{Bout}$			−0.6	2.34
$\log K_{B-out}$			−10.0	
C_1			1.31 [b]	1.0
C_2			0.2 [b]	1.0
WSOS/DF	6.9	0.8	11.6	1.7

Surface site densities are equal to 4.53 and 2.54 sites/nm^2 for goethite and birnessite, respectively. Specific surface areas are equal to 20 and 29 m^2/g for goethite and birnessite, respectively. C_1 and C_2 are the capacitance values (F/m^2) of the inner-sphere and the outer-sphere complexes, respectively. Other calculated constants are defined in Appendix A.

[a] Values taken from Sverjensky (2005).

[b] Values taken from Balistrieri and Murray (1982).

4.1.2. Birnessite

Because our DRIFT spectroscopy study clearly supports the presence at birnessite surface of both outer-sphere and inner-sphere complexes, we modeled boron sorption within the framework of the triple layer model (TLM). In this model, we also considered the formation of an inner-sphere tetrahedral boron complex probably hidden from DRIFT probe by birnessite Mn–OH vibration bands.

In a first attempt, values of surface protonation/deprotonation constants and TLM capacitances values were taken from Balistrieri and Murray (1982) and only boron surface speciation constants were fitted. In a second attempt, surface capacitance values and all speciation constants were simultaneously fitted. In both models, birnessite surface site density was taken from the results of boron adsorption isotherm performed in this study (2.54 sites/nm^2). Model parameters values are listed in Table 2 and boron surface speciations obtained as function of pH are illustrated in Fig. 5-C and D. The

first model (Fig. 5-C) provides a poor fit of experimental data at pH < 9 and could not account for the presence of trigonal inner-sphere complexes evidenced by infrared spectroscopy. The second model (Fig. 5-D), consistent with DRIFT observations, accurately describes boron experimental sorption with the following values of birnessite interfacial parameters: $C_1 = 1.0$ F/m^2, $C_2 = 1.0$ F/m^2, $pKa_1 = 7.25$ and $pKa_2 = 10.43$. The derived high value for birnessite point of zero charge (pH_{ZPC}) may originate from the very poor crystallinity of our birnessite and non dissociative water physisorption resulting in high protonation constants (Prelot et al., 2003b). According to this second model, a trigonal inner-sphere complex forms at acid pH conditions, and trigonal outer-sphere and tetrahedral inner-sphere complexes dominate boron surface speciation at pH > 7.

4.2. Isotopic modeling

In agreement with the Lemarchand et al. (2005) study of boron isotopic fractionation during adsorption on humic acid, a specific fractionation factor $\alpha_{Boxy\text{-}III}$ was assumed between each type of boron complex present at the goethite or birnessite surface and aqueous boric acid. Knowing the distribution of boron aqueous and surface species, fitting of Eq. (3) by a least square method allows determination of the values of the different $\alpha_{Boxy\text{-}III}$ fractionation factors. For this purpose, accurate knowledge of boron isotope fractionation factor between borate ion and boric acid (α_{IV-III}) is a keystone. The earliest and most widely used estimation for α_{IV-III} ($\alpha_{IV-III} = 0.9810$ at 25 °C) is that of Kakihana et al. (1977) which is based on reduced partition function ratio calculations from spectroscopic data on molecular vibrations. This value has been recently confirmed by Sanchez-Valle et al. (2005) based on the same spectroscopic approach. However, recent and more rigorous theoretical treatment of the spectroscopic data using *ab initio* molecular orbital theory (Oi et al., 2000; Oi, 2001; Liu and Tossell, 2005) and direct experimental evaluation of B(III)–B(IV) isotopic equilibrium (Byrne et al., 2006; Klochko et al., 2006) indicated significantly lower α_{IV-III} values (ranging from

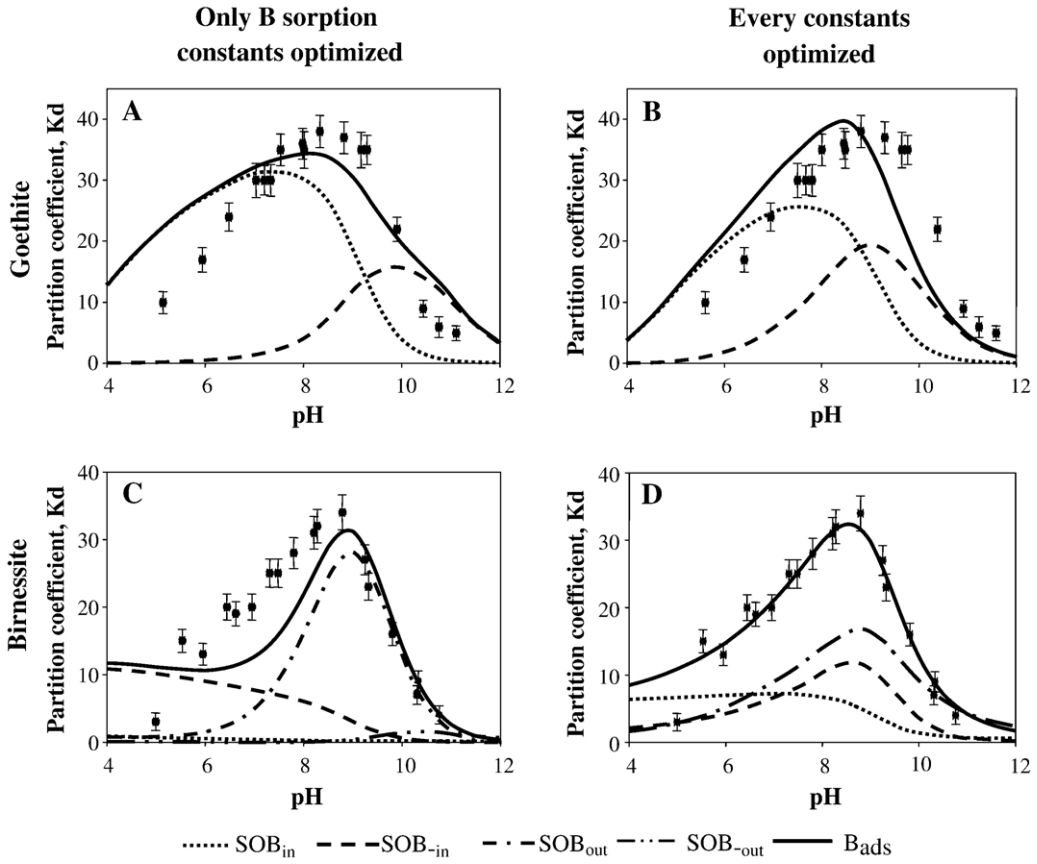

Fig. 5. Modeling of boron sorption at the surface of goethite (A–B) and birnessite (C–D) at 25 °C and $I = 0.1$ M. Symbols represent experimental data but solid lines represent calculated Kd values. Values of models parameters are listed in Table 2.

Table 3
Different structures expected for boron complexes present at the surface of goethite and birnessite and corresponding isotopic fractionation factors

Solid	Structure of adsorbed boron complexes	Isotopic fractionation factor relative to $B(OH)_{3,aq}$	
Goethite	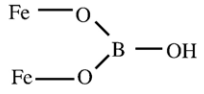	$\alpha_{Bin\text{-}III}$	0.959
	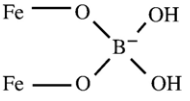	$\alpha_{B^-\ in\text{-}III}$	0.966
Birnessite	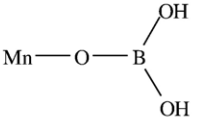	$\alpha_{Bin\text{-}III}$	1.001
	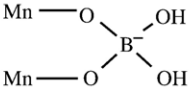	$\alpha_{B^-\ in\text{-}III}$	0.945
	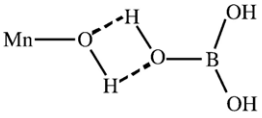	$\alpha_{Bout\text{-}III}$	1.002

0.976 to 0.968 at 25 °C). In the present study, isotopic modeling was performed using $\alpha_{IV-III}=0.970$, which is the experimental value determined at 25 °C in pure water by Klochko et al. (2006).

4.2.1. Goethite

Calculated values of individual fractionation factors of boron surface species are listed in Table 3, whereas calculated boron isotope fraction factor between solution and goethite surface is plotted as a function of solution pH and compared to experimental values in Fig. 6-A. It can be seen that the goethite surface speciation model provides an accurate fit of experimental data and plausible values of the isotopic fractionation factor α_i which is distinctly lower for surface trigonal ($\alpha_{Bin\text{-}III}=0.959$, $\Delta=-42‰$) than for surface tetrahedral complexes ($\alpha_{B-in\text{-}III}=0.966$, $\Delta=-35‰$).

4.2.2. Birnessite

Predicted values of individual boron isotopes fractionation factors are listed in Table 3, while calculated fractionation factor between solution and birnessite surface is plotted as a function of pH and compared to its experimental counterpart in Fig. 6-B. It can be seen that the birnessite surface speciation model provides both likely α_i values and an accurate fit of experimental data on the overall pH range. Strong isotopic fractionation is calculated between aqueous boric acid and inner-sphere tetrahedral boron surface complex ($\alpha_{B-in\text{-}III}=0.945$, $\Delta=-57‰$) which is consistent with the steric strains induced by the formation of a bidendate binuclear complex on metal oxide surface. As could be expected, the isotopic composition of the monodendate outer-sphere and inner-sphere trigonal complexes are close to that of aqueous boric acid ($\alpha_{Bout\text{-}III}=1.002$, $\Delta=+2‰$; $\alpha_{Bin\text{-}III}=1.001$, $\Delta=+1‰$).

5. Discussion

5.1. Boron isotopic fractionation and the structure of boron surface complexes

The combination of the various macroscopic, spectroscopic and modeling techniques used in this study provides important insights on the mechanisms that control boron sorption on metal oxides and its related isotopic fractionation. The different structures expected for boron complexes and their isotopic composition are presented in Table 3.

Boron appears to only form inner-sphere complexes with goethite. Trigonal inner-sphere complexes are easily detected on DRIFT spectra, whereas the formation of tetrahedral complexes, if not clearly evidenced by infrared spectroscopy, cannot be rejected as the characteristic ~940 cm^{-1} band of these complexes is likely to be hidden in the strong goethite Fe–OH vibration band at 800 to 1000 cm^{-1}. Moreover, two infrared studies (Su and Suarez, 1995; Peak et al., 2003) have evidenced the formation of such tetrahedral complexes on amorphous ferric oxide which does not exhibit the metal oxide vibration band.

The formation of bidendate binuclear complexes on goethite surface is likely to be responsible for the surprisingly light isotopic composition of the trigonal complex ($\alpha_{Bin\text{-}III}=0.959$) compared to the tetrahedral one ($\alpha_{B-in\text{-}III}=0.966$). Although infrared spectroscopy is not capable of distinguishing monodendate from bidendate surface boric acid, Peak et al. (2003) have proposed reaction pathways that explain the conversion from monodendate to bidendate of both trigonal and tetrahedral boron sorbed on amorphous iron hydroxide. The formation of bidendate binuclear boron complexes on goethite surface is further supported by the XAFS spectroscopy evidence of the formation of bidendendate silicic and arsenious acids complexes on the corners of

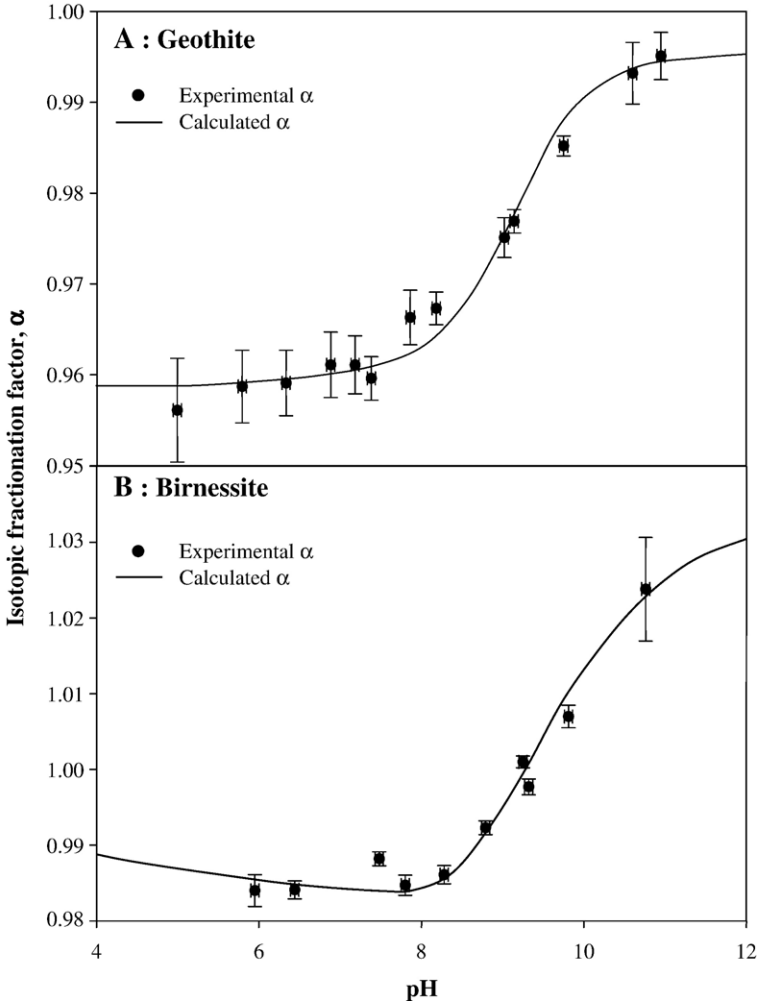

Fig. 6. Modeling (solid line) at 25 °C and I=0.1 M of sorption dependent boron isotopic fractionation on goethite (A) and birnessite (B). Corresponding adsorption models are those where every constants were optimized (see Table 2 and Fig. 5). Values of B isotopic fractionations factors are listed in Table 3. Calculations were performed with α_{IV-III}=0.970.

FeO_6− octahedra (Farquhar et al., 2002; Manning et al., 1998; Pokrovski et al., 2003). The formation of such trigonal boron bidendate complexes induces strong steric strains as demonstrated by simple geometric considerations. In aqueous solution, the OBO angle is equal to 120 and 109° for boric acid and borate ion, respectively. The maximum length found for B–O bounds in solids is 1.403 and 1.512 Å for trigonal and tetrahedral boron, respectively (Hawthorne et al., 2002). With these values of B–O bond lengths and OBO angles, the maximum distance between two oxygen atoms is 2.430 and 2.462 Å for B(III) and B(IV), respectively. As the shortest distance between two oxygen atoms at goethite surface is equal to 2.593 Å (Szytula et al., 1968), formation of bidendate binuclear complexes should yield an increase of the OBO angle of 15 and 9° in trigonal and tetragonal boron complexes, respectively. Thus, the formation of highly distorted bidendate structures is likely to account for the very light isotopic composition of sorbed trigonal boron as ^{11}B should concentrate in the species in which it is more strongly bonded (Criss, 1999).

The presence of both inner- and outer-sphere B complexes at birnessite surface can account for the isotopic composition of sorbed boron as a function of pH. Both trigonal inner- and outer-sphere complexes can be clearly distinguished on infrared spectra whereas, as in the case of goethite, inner-sphere tetrahedral complex are probably hidden by birnessite Mn–OH vibration band at 920 cm^{-1}. Tetrahedral inner-sphere complexes are strongly enriched in light boron ($\alpha_{B-in-III}$=0.945), whereas the isotopic compositions of both trigonal inner-sphere and outer-sphere complexes are close to that of boric acid ($\alpha_{Bin-III}$=

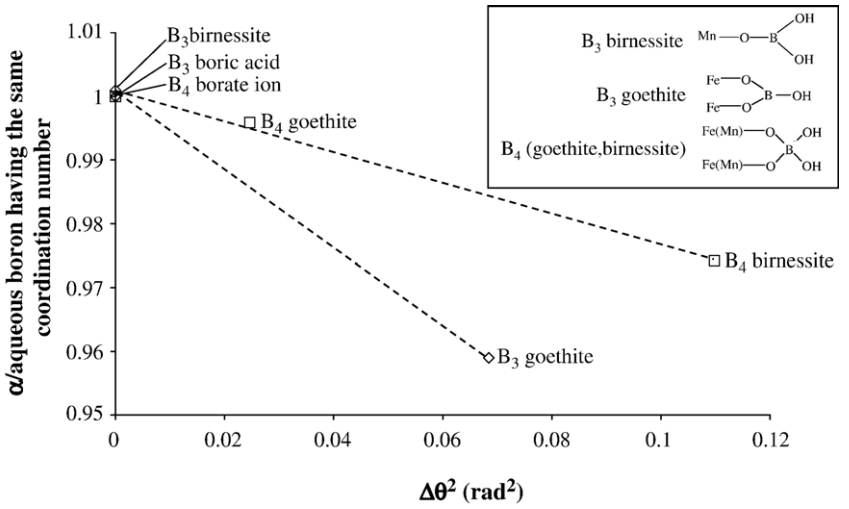

Fig. 7. Plot of B isotopic fractionation factor between boron surface and aqueous species having the same coordination number as a function of $\Delta\theta^2$. $\Delta\theta$ represents the variation of the OBO angle in a given B aqueous species induced by its sorption onto goethite or birnessite (see text).

1.001, $\alpha_{\text{Bout-III}}=1.002$). In birnessite, unlike in goethite, the long distance between two surface oxygen atoms (2.70 Å as deduced from a Mn–O distance of 1.92 Å in Na–birnessite (Silvester et al., 1997) prevents the formation of trigonal bidendate binuclear complexes. As a result, boron is likely to form trigonal monodendate inner-sphere complexes with an isotopic composition close to that of boric acid but much heavier than that of the trigonal bidendate complexes formed at goethite surface. Likewise, the formation of boron trigonal outer-sphere complexes, very similar to aqueous boric acid, is consistent with the very small isotopic fractionation predicted between these complexes and boric acid ($\alpha_{\text{Bout-III}}=1.002$). The higher length of the B–O bounds in tetrahedral boron allows the formation at birnessite surface of tetrahedral bidendate binuclear complexes, but with an increase of the OBO angle of at least 19°, which results in a very light isotopic composition of this complex ($\alpha_{\text{B-in-III}}=0.945$, $\Delta=-57‰$). It should be emphasized that, within the framework of this surface complexation scheme, it is the formation of isotopically heavy trigonal outer-sphere (and, to a lesser extent, inner-sphere) complexes that is responsible for the heavier isotopic composition of birnessite boron than goethite boron both at acid and alkaline pH.

The effect of angle deformation on the energy (and thus isotopic composition) of boron surface complexes can be approximated from simple molecular mechanic considerations. The energy associated with valence angle deformation can be described in terms of an harmonic oscillator (Brubaker and Johnson, 1984):

$$U_\theta = 1/2K_\theta(\theta_i - \theta_0)^2 \quad (6)$$

where K_θ stands for the deformation angle constant and θ_i is the OBO angle in the considered boron surface complex and θ_0 is the unstrained angle (in corresponding boron aqueous complex). Plot, as a function of $\Delta\theta^2$ (with $\Delta\theta=\theta_i-\theta_0$), of B isotopic fractionation factor between boron surface and aqueous species having the same coordination number yields, in accordance with Eq. (6), a nice linear correlation (Fig. 7) which confirms the strong impact of steric strains on the isotopic composition of boron species sorbed onto goethite and birnessite.

5.2. Geological applications

The results obtained in this study have several implications for the boron cycle at the surface of the Earth.

1. In the pH range of natural waters, significant boron isotopes fractionation will occur during the interaction of soil solutions with oxide surfaces. Boron isotopes can therefore be used as a proxy for pH in paleosoils or sediments. It should be stressed at that point that the mechanisms studied here only concern adsorption and not coprecipitation which may be an additional natural mechanism for boron incorporation in minerals. However, because boron coprecipitation with Fe and Mn hydroxides should proceed through the formation of the same surface complexes, it is likely that related isotope fractionations are similar to those generated by adsorption. This is confirmed by results of the study of Sen et al. (1994) of the coordination environment and isotope composition of B impurities in calcite and aragonite that

showed B isotopes compositions to be the same in both minerals despite the preponderance of B(III) in calcite (with 20% B(IV)) but the only presence of B (IV) in aragonite. In addition, the markedly different isotopic fractionation factor, at the same pH, of boron sorbed on goethite and birnessite (at pH=8.2, α is equal to 0.967 and 0.986 for goethite and birnessite, respectively) may be used to determine past pH values without requiring knowledge of water past isotopic composition, as well in paleosoils and sediments, as in the ocean.

2. Our findings also have implications for modern soil systems. Several authors have advocated a strong impact of continental weathering on boron chemical and isotopic budget (Spivack et al., 1987; Lemarchand et al., 2002; Rose et al., 2002). For example, Rose et al. (2002) in a study of the isotopic composition of Himalayan rivers indicate that boron adsorption processes in soils may significantly affect its isotopic composition in rivers. It has been noted by Lemarchand et al. (2002) in their global systematics of large rivers that tropical waters are systematically enriched in ^{11}B compared to continental crust. The results of this study do show that adsorption of boron onto Fe oxides is a significant process affecting the boron isotopic composition of soil and river waters. As a sensitivity test, we attempted to quantify the impact of boron sorption onto oxides in tropical soils by taking two extreme granitic weathering styles represented by the Nsimi (Cameroon) and the Rio Icacos (Puerto Rico) watersheds. Both have been the subject of extensive studies (Oliva et al., 1999; White et al., 1998). Total denudation rate of the Nsimi watershed are about 5 mm/kyr, with a ratio of chemical over physical erosion fluxes about unity. The Rio Icacos displays chemical weathering rates ~10 times those of Nsimi watershed. In both watersheds, goethite is recognized to be the dominant Fe-bearing phase (5% at Nsimi and 3.4% at R. Icacos). Expressing boron mass and isotope conservation yields the following expression for boron isotopic fractionation between bed rocks and soil solution ($\Delta_{w\text{-}rock}$) as a function of the water/iron oxide ratio (W_R):

$$\Delta_{w-rock}(‰) = \frac{Kd(1-\alpha)}{\alpha Kd + W_R} \quad (7)$$

with Kd and α the partition coefficient and isotopic fractionation factor between solution and iron oxides, respectively. In Cameroon and Puerto Rico, soil porosity and density are typically 40–50% and 2.7 g/cm^3, respectively, which lead to typical water–rock ratios of 0.3–0.5 mL/g and hence water–Fe oxides ratios of 5–10. The isotopic shift induced by B sorption on Fe oxides at pH 5 (Nsimi) and 7 (Icacos) is shown on Fig. 8 as a function of the water/iron oxide ratio. It clearly shows that this process can significantly influence the soil solution isotopic composition. Like organic matter (Lemarchand et al., 2005), iron oxides may thus be largely responsible for the heavy ^{11}B compositions exhibited by tropical rivers (Amazon: 15.1‰, Congo: 28.4‰, Niger: 35.2‰ (Lemarchand et al., 2002)).

3. The third consequence that emerges from the above experimental study concerns the boron oceanic cycle. A substantial flux of Fe oxides are added to the ocean each year. In a recent paper, Raiswell et al. (2006) revisited the global iron oxyde cycle by using new estimates of Fe oxide concentration in the different source materials (Raiswell et al., 2006). The sources of Fe oxides to the ocean are the riverine inputs (containing a few % of highly reactive Fe in the form of oxides), the glacial flux (0.5% Fe in particulates), Aeolian dusts (1% of oxide Fe), costal erosion, diagenetic recycling and hydrothermal inputs. Based on these new estimates, the total flux of oxide Fe is calculated to be 315–470.10^{12} g/yr. In glacial sediments, Fe oxides are present in the form of nano-particles.

Based on the above results we calculate that the adsorption of seawater boron onto these oxides at pH=8.3 (Kd=40, ionic strengh of 0.1 M) would result in an annual flux of 6–8×10^{10} gB fixed on Fe oxide surfaces. The flux of boron scavenged at the surface of marine sediments was estimated to be 13×10^{10} gB/yr (Spivack

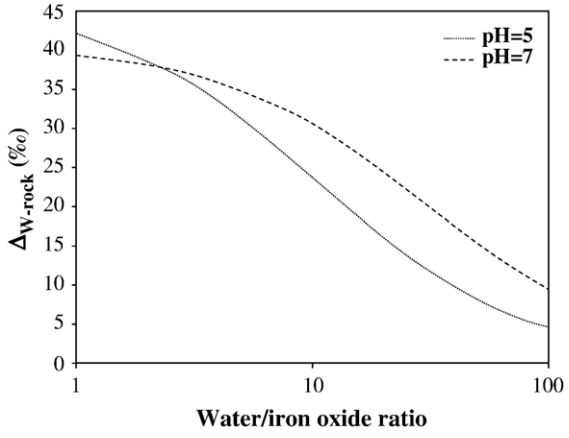

Fig. 8. Calculated B isotopic fractionation between bed rocks and soil solution ($\Delta_{\varphi\text{-}rock}$) as a function of the water/iron oxide ratio (W_R) in the Nsimi and Rio Icacos watersheds using Kd and α values determined in this study for B sorption on goethite surface at pH=5 (Nsimi) and pH=7 (Rio Icacos).

et al., 1987) based on the annual sedimentary flux to the ocean. The number calculated here therefore shows that about half of boron scavenging in seawater could be due to oxide surfaces. The bulk fractionation factor determined for the sorption of boron onto suspended sediments by (Spivack et al., 1987) was −25‰ based on experiments using sediments from the Mississippi. The important fractionations related to sorption onto oxides that we found in this paper show that a substantial part of this fractionation can be attributed to oxides. The role of oxides in the marine boron cycle is thus considerable and the oxidation events that occurred during the Early Earth history may have had a significant influence on the evolution of boron in the ocean by adding to the ocean new surfaces with a high boron affinity.

6. Conclusion

The present study presents several important implications for the mechanism of boron sorption onto oxide surfaces and its subsequent isotopic fractionation.

1. Boron adsorption on goethite and birnessite at 25 °C is pH-dependent, with a typical anionic sorption bell-shaped curve. Maximum boron sorption occurs at $8<pH<9$ with Kd values of 40 and 35 for goethite and birnessite, respectively, that are higher than corresponding values for clay minerals and humic acids.
2. This study demonstrates for the first time that B sorption on metal oxides strongly fractionates boron isotopes. Isotopic fractionation is pH-dependent and particularly important during sorption on goethite with ^{10}B enrichment on the solid surface ($\alpha_{oxy\text{-}solution}=0.96$, $\Delta=-40‰$ at $pH<8$). B isotopic fractionation is less substantial during sorption on birnessite at $pH<8.5$ ($\alpha_{oxy\text{-}solution}=0.985$, $\Delta=-15‰$) but it reverses at $pH>9$ and leads to a strong enrichment of birnessite surface in ^{11}B ($\alpha_{oxy\text{-}solution}=1.023$, $\Delta=+23‰$ at $pH=10.8$). To our knowledge, it is the first time that enrichment in ^{11}B is found to follow boron sorption on inorganic or organic surfaces.
3. B isotopic fractionation arises because the speciation and structure of adsorbed boron is always quite different from those of boron in aqueous solution. Steric strains induced by the formation of a trigonal bidendate binuclear complex are responsible for the strong enrichment in ^{10}B at the surface of goethite, whereas the formation of a B trigonal outer-sphere complex causes the enrichment of birnessite surface in ^{11}B at $pH>9$.
4. Together with the recent characterization of boron isotopic fractionation induced by its interaction with organic matter (Lemarchand et al., 2005), this study demonstrates that boron isotopic composition can be deeply altered during weathering processes occurring both on continental surfaces and in the oceans. For example, we calculated that iron oxide surfaces can be responsible of about half of the boron flux scavenged by marine sediments, which could significantly impact the isotopic composition of seawater boron. The rigorous interpretation of boron isotopes cycles at the earth surface, however, will require both more experimental data on B interactions with inorganic, organic and biologic surfaces, and inputs from quantum mechanical methods to rigorously determine the free energy of the various boron isotopomers formed during these interactions. In the meantime, boron isotopic data in soils are deeply needed.

Acknowlegments

This study was supported by Programme National de Recherches Sols et Erosion (PNSE) of CNRS and by a PhD fellowship to E. L. from the French Ministère de l'Enseignement et de la Recherche. DRIFT analyses were performed by Odile Barres at LEM, UMR 7569, INPL-ENSG, Vandoeuve-les-Nancy, France. Jocelyne Escalier, Carole Causserand and Stephanie Levet are thanked for performing flame absorption spectroscopic analyses and for their help with colorimetric analyses; Michel Thibault is thanked for performing XRD and thermo gravimetric analyses. We also would like to thank Oleg Pokrovsky for his advices in the design of sorption experiments, and Damien Lemarchand and Benjamin Chetelat for help with isotopic analyses and helpful discussions. This paper was greatly improved by the constructive comments of Pr. Claude P. Jaupart and an anonymous reviewer. This is CNRS-INSU-PNSE and IPGP contributions no. 403 and no. 2232, respectively.

Appendix A. Chemical reactions used in the FITEQL modeling

Aqueous reactions

$$B(OH)_3 + H_2O \rightarrow B(OH)_4^- + H^+,$$
$$Ka_B = \frac{(B(OH)_4^-)\cdot(H^+)}{(B(OH)_3)}$$

$$Na^+ + B(OH)_4^- \rightarrow NaB(OH)_4^0,$$
$$K_{NaB} = \frac{(NaB(OH)_4^0)}{(Na^+)\cdot(B(OH)_4^-)}$$

Surface protonation/deprotonation

$$\mathrm{SOH} \rightarrow \mathrm{SO^-} + \mathrm{H^+},$$
$$\mathrm{Ka_1} = \frac{[\mathrm{SO^-}] \cdot (\mathrm{H^+})}{[\mathrm{SOH}]} \exp(-F\Psi_0/RT)$$

$$\mathrm{SOH} + \mathrm{H^+} \rightarrow \mathrm{SOH_2^+},$$
$$\mathrm{Ka_2} = \frac{[\mathrm{SOH_2^+}]}{[\mathrm{SOH}] \cdot (\mathrm{H^+})} \exp(F\Psi_0/RT)$$

Formation of boron trigonal and tetragonal inner-sphere surface complexes

$$\mathrm{SOH} + \mathrm{B(OH)_3} \rightarrow \mathrm{SOB(OH)_2},$$
$$K_{\mathrm{Bin}} = \frac{[\mathrm{SOB(OH)_2}]}{[\mathrm{S(OH)}] \cdot (\mathrm{B(OH)_3})}$$

$$\mathrm{SOH} + \mathrm{B(OH)_3} \rightarrow \mathrm{SOB(OH)_3^-} + \mathrm{H^+},$$
$$K_{\mathrm{B^-in}} = \frac{[\mathrm{SOB(OH)_3^-}] \cdot (\mathrm{H^+})}{[\mathrm{S(OH)}] \cdot (\mathrm{B(OH)_3})} \exp(-F\Psi_0/RT)$$

Formation of corresponding outer-sphere complexes

$$\mathrm{SOH} + \mathrm{B(OH)_3} \rightarrow \mathrm{SOH_2^+ - BO(OH)_2^-},$$
$$K_{\mathrm{Bout}} = \frac{[\mathrm{SOH_2^+ - BO(OH)_2^-}]}{[\mathrm{S(OH)}] \cdot (\mathrm{B(OH)_3})} \exp[F(\Psi_0 - \Psi_\beta)/RT]$$

$$\mathrm{SOH} + \mathrm{B(OH)_3} + \mathrm{OH^-} \rightarrow \mathrm{SOH_2^+ - BO(OH)_3^{2-}},$$
$$K_{\mathrm{B^-out}} = \frac{[\mathrm{SOH_2^+ - BO(OH)_3^{2-}}]}{[\mathrm{SOH}] \cdot (\mathrm{B(OH)_3}) \cdot (\mathrm{OH^-})} \times \exp[F(\Psi_0 - 2\Psi_\beta)/RT]$$

$$\mathrm{SOH} + \mathrm{Na^+} \rightarrow \mathrm{SO^- - Na^+} + \mathrm{H^+},$$
$$K_{\mathrm{Na^+}} = \frac{[\mathrm{SO^- - Na^+}] \cdot (\mathrm{H^+})}{[\mathrm{SOH}] \cdot (\mathrm{Na^+})} \exp[F(\Psi_\beta - \Psi_0)/RT]$$

[*i*] (mol/L) represents the concentration of species *i*, (*i*) is the activity of *i*, *F* (C/mol) stands for the Faraday constant, *R* (J/mol/K) represents the gas constant, *T*(K) is the absolute temperature and Ψ_0 and Ψ_β (V) stands for the inner-sphere and outer-sphere surface potentials, respectively.

References

Abou-El-Sherbini, K.S., Askar, M.H., Schollhorn, R., 2002. Hydrated layered manganese dioxide: Part I. Synthesis and characterization of some hydrated layered manganese dioxides from [alpha]-$NaMnO_2$. Solid State Ionics 150, 407–415.

Anovitz, L.M., Grew, E.S., 2002. Mineralogy, petrology and geochemistry of boron: an introduction. In: Grew, E.S., Anovitz, L.M. (Eds.), Boron: Mineralogy, Petrology and Geochemistry. Mineralogical Society of America, pp. 1–40.

Baes, C.F., Mesmer, R.E., 1976. The Hydrolysis of Cations. Wiley, New York.

Balistrieri, L.S., Murray, J.W., 1982. The surface chemistry of δMnO_2 in major ion seawater. Geochim. Cosmochim. Acta 46, 1041–1052.

Barth, S., 1993. Boron isotope variations in nature: a synthesis. Int. J. Earth Sci. 82, 640–651.

Brubaker, G.R., Johnson, D.W., 1984. Molecular mechanics calculations in coordination chemistry. Coord. Chem. Rev. 53, 1–36.

Byrne, R.H., Yao, W., Klochko, K., Tossell, J.A., Kaufman, A.J., 2006. Experimental evaluation of the isotopic exchange equilibrium $^{10}B(OH)_3 + {}^{11}B(OH)_4^- = {}^{11}B(OH)_3 + {}^{10}B(OH)_4^-$ in aqueous solution. Deep-Sea Res., Part 1, Oceanogr. Res. Pap. 53, 684–688.

Capelle, K., 1961. Microdosage colorimétrique du bore en milieu aqueux, au moyen de réactifs à groupement azoïque ou imine dérivés des acides H et K. Anal. Chim. Acta 24, 555–572.

Criss, R.E., 1999. Principles of Stable Isotope Distribution. Oxford University Press, Oxford.

de Bussetti, S.G., Ferreiro, E.A., Helmy, A.K., 1995. Sorption of boron by hydrous Al-oxide. Clays Clay Miner. 43, 58–62.

Farquhar, M., Charnock, L.J.M., Livens, F.R., Vaughan, D.J., 2002. Mechanisms of arsenic uptake from aqueous solution by interaction with goethite, lepidocrocite, mackinawite, and pyrite: an X-ray absorption spectroscopic study. Environ. Sci. Technol. 36, 1757–1762.

Gaillardet, J., Lemarchand, D., Göpel, C., Manhès, G., 2001. Evaporation and sublimation of boric acid: application for boron purification from organic rich solutions. Geostand. Newsl. 25, 67–75.

Goldberg, S., 1985. Chemical modeling of anion competition on goethite using the constant capacitance model. Soil Sci. Soc. Am. J. 49, 851–856.

Goldberg, S., 1999. Reanalysis of boron adsorption on soils and soil minerals using the constant capacitance model. Soil Sci. Soc. Am. J. 63, 823–829.

Goldberg, S., 2005. Inconsistency in the triple layer model description of ionic strength dependent boron adsorption. J. Colloid Interface Sci. 285, 509–517.

Goldberg, S., Glaubig, R.A., 1985. Boron adsorption on aluminium and iron oxide minerals. Soil Sci. Soc. Am. J. 49, 1374–1379.

Goldberg, S., Glaubig, R.A., 1986a. Boron adsorption and silicon release by the clay minerals kaolinite, montmorillonite, and illite. Soil Sci. Soc. Am. J. 50, 1442–1446.

Goldberg, S., Glaubig, R.A., 1986b. Boron adsorption on California soils. Soil Sci. 50, 1173–1176.

Goldberg, S., Glaubig, R.A., 1988. Boron and silicon adsorption on an aluminium oxide. Soil Sci. Soc. Am. J. 52, 87–91.

Goldberg, S., Forster, H.S., Heick, E.L., 1993. Temperature effects on boron adsorption by reference minerals and soils. Soil Sci. 156, 316–321.

Goldberg, S., Lesch, S.M., Suarez, D.L., 2000. Predicting boron adsorption by soils using soil chemical parameters in the constant capacitance model. Soil Sci. Soc. Am. J. 64, 1356–1363.

Gu, B., Lowe, L.E., 1990. Studies on the adsorption of boron on humic acids. Can. J. Soil Sci. 70, 305–311.

Hawthorne, F.C., Burns, P.C., Grice, J.D., 2002. The crystal chemistry of boron. In: Grew, E.S., Anovitz, L.M. (Eds.), Boron: Mineralogy, Petrology and Geochemistry. Mineralogical Society of America, pp. 41–116.

Hemming, N.G., Hanson, G.N., 1992. Boron isotopic composition and concentration in modern marine carbonates. Geochim. Cosmochim. Acta 56, 537–543.

Hemming, N.G., Reeder, R.J., Hanson, G.N., 1995. Mineral-fluid partitioning and isotopic fractionation of boron in synthetic calcium carbonate. Geochim. Cosmochim. Acta 59, 371–379.

Herbelin, A., Westall, J.C., 1996. FITEQL: A computer program for determination of chemical equilibrium constants from experimental data. Department of Chemistry, Oregon State University, Corvallis.

Kakihana, H., Kotaka, M., Satoh, S., Nomura, M., Okamoto, M., 1977. Fundamental studies on the ion-exchange separation of boron isotopes. Bull. Chem. Soc. Jpn. 50, 158–163.

Keren, R., Gast, R.G., 1983. pH-dependent boron adsorption by montmorillonite hydroxy–aluminium complexes. Soil Sci. Soc. Am. J. 47, 1116–1121.

Keren, R., Mezuman, U., 1981. Boron adsorption by clay minerals using a phenomenological equations. Clays Clay Miner. 29, 198–204.

Keren, R., Gast, R.G., Bar-Yosef, B., 1981. pH-dependence boron adsorption by Na–montmorillonite. Soil Sci. Soc. Am. J. 45, 45–48.

Klochko, K., Kaufman, A.J., Yao, W., Byrne, R.H., Tossell, J.A., 2006. Experimental measurement of boron isotope fractionation in seawater. Earth Planet. Sci. Lett. 248, 261–270.

Lemarchand, D., Gaillardet, J., 2006. Transient features of the erosion of shales in the Mackenzie basin (Canada), evidences from boron isotopes. Earth Planet. Sci. Lett. 245, 174–189.

Lemarchand, D., Gaillardet, J., Lewin, E., Allegre, C.J., 2002. Boron isotope systematics in large rivers: implications for the marine boron budget and paleo-pH reconstruction over the Cenozoic. Chem. Geol. 190, 123–140.

Lemarchand, E., Schott, J., Gaillardet, J., 2005. Boron isotopic fractionation related to boron sorption on humic acid and the structure of surface complexes formed. Geochim. Cosmochim. Acta 69, 3519–3533.

Lemarchand, D., Gaillardet, J., Gopel, C., Manhes, G., 2002. An optimized procedure for boron separation and mass spectrometry analysis for river samples. Chem. Geol. 182, 323–334.

Liu, Y., Tossell, J.A., 2005. Ab initio molecular orbital calculations for boron isotope fractionations on boric acids and borates. Geochim. Cosmochim. Acta 69, 3995–4006.

Loganathan, P., Bureau, R.G., Fuerstenau, D.W., 1977. Influence of pH on the sorption of Co^{2+}, Zn^{2+} and Ca^{2+} by a hydrous manganese oxide. Soil Sci. Soc. Am. J. 41, 57–62.

Manning, B.A., Fendorf, S.E., Goldberg, S., 1998. Surface structures and stability of arsenic (III) on goethite: spectroscopic evidence for inner-sphere complexes. Environ. Sci. Technol. 32, 2383–2388.

Oliva, P., Viers, J., Dupre, B., Fortune, J.P., Martin, F., Braun, J.J., Nahon, D., Robain, H., 1999. The effect of organic matter on chemical weathering: study of a small tropical watershed: Nsimi-Zoetele site, Cameroon. Geochim. Cosmochim. Acta 63, 4013–4035.

Oi, T., 2000. Calculations of reduced partition function ratios of monomeric and dimeric boric acids and borates by the ab initio molecular orbital theory. J. Nucl. Sci. Technol. 37, 166–172.

Oi, T., 2001. Calculations of reduced partition function ratios of hydrated monoborate anion by the ab initio molecular orbital theory. J. Nucl. Sci. Technol. 38, 429–432.

O'Neil, J.R., 1986. Theoretical and experimental aspects of isotopic fractionation. In: Valley, J.W., Taylor, H.P.J., O'Neil, J.R. (Eds.), Stable Isotopes in High Temperature Geological Processes. Mineralogical Society of America, pp. 1–40.

Pagani, M., Lemarchand, D., Spivack, A., Gaillardet, J., 2005. A critical evaluation of the boron isotope-pH proxy: the accuracy of ancient ocean pH estimates. Geochim. Cosmochim. Acta 69, 953–961.

Palmer, M.R., Spivack, A.J., Edmond, J.M., 1987. Temperature and pH controls over isotopic fractionation during adsorption of boron on marine clay. Geochim. Cosmochim. Acta 51, 2319–2323.

Peak, D., Luther III, G.W., Sparks, D.L., 2003. ATR-FTIR spectroscopic studies of boric acid adsorption on hydrous ferric oxide. Geochim. Cosmochim. Acta 67, 2551–2560.

Pokrovski, G.S., Schott, J., Sergeyev, A.S., 1995. Experimental determination of the stability constants of $NaSO_4^-$ and $NaB(OH)_4^0$ in hydrothermal solutions using a new high-temperature sodium-selective glass electrode—implications for boron isotopic fractionation. Chem. Geol. 124, 253–265.

Pokrovski, G.S., Schott, J., Farges, F., Hazemann, J.-L., 2003. Iron (III)–silica interactions in aqueous solution: insights from X-ray absorption fine structure spectroscopy. Geochim. Cosmochim. Acta 67, 3559–3573.

Prelot, B., Villieras, F., Pelletier, M., Gerard, G., Gaboriaud, F., Ehrhardt, J.-J., Perrone, J., Fedoroff, M., Jeanjean, J., Lefevre, G., 2003a. Morphology and surface heterogeneities in synthetic goethites. J. Colloid Interface Sci. 261, 244–254.

Prelot, B., Poinsignon, C., Thomas, F., Schouller, E., Villieras, F., 2003b. Structural-chemical disorder of manganese dioxides: 1. Influence on surface properties at the solid–electrolyte interface. J. Colloid Interface Sci. 257, 77–84.

Raiswell, R., Tranter, M., Benning, L.G., Siegert, M., De'ath, R., Huybrechts, P., Payne, T., 2006. Contributions from glacially derived sediment to the global iron (oxyhydr)oxide cycle: implications for iron delivery to the oceans. Geochim. Cosmochim. Acta 70, 2765–2780.

Rose, E.F., Chaussidon, M., France-Lanord, C., 2000. Fractionation of boron isotopes during erosion processes: the example of Himalayan rivers. Geochim. Cosmochim. Acta 64, 397–408.

Ruan, H.D., Frost, R.L., Kloprogge, J.T., Duong, L., 2002. Infrared spectroscopy of goethite dehydroxylation: III. FT-IR microscopy of in situ study of the thermal transformation of goethite to hematite. Spectrochim. Acta, Part A: Mol. Biomol. Spectrosc. 58, 967–981.

Sanchez-Valle, C., Reynard, B., Daniel, I., Lecuyer, C., Martinez, I., Chervin, J.-C., 2005. Boron isotopic fractionation between minerals and fluids: new insights from in situ high pressure-high temperature vibrational spectroscopic data. Geochim. Cosmochim. Acta 69, 4301–4313.

Sanyal, A., Hemming, N.G., Broecker, W.S., Lea, D.W., Spero, H.J., Hanson, G.N., 1996. Oceanic pH control on the boron isotopic composition of foraminifera: evidence from culture experiments. Paleoceanography 11, 513–517.

Sanyal, A., Nugent, N., Reeder, R.J., Bijma, J., 2000. Seawater pH control on the boron isotopic composition of calcite: evidence from inorganic calcite precipitation experiments. Geochim. Cosmochim. Acta 64, 1551–1555.

Schauble, E.A., 2004. Applying stable isotope fractionation theory to new systems. In: Johnson, C.M., Beard, B.L., Albarede, F. (Eds.), Geochemistry of Non-Traditional Stable Isotopes. Mineralogical Society of America, pp. 65–111.

Schwarcz, H., Agyei, E., McMullen, C., 1969. Boron isotopic fractionation during clay adsorption from seawater. Earth Planet. Sci. Lett. 6, 1–5.

Sen, S., Stebbins, J.F., Hemming, N.G., Ghosh, B., 1994. Coordination environments of B impurities in calcite and aragonite polymorphs: a ^{11}B MAS NMR study. Am. Mineral. 79, 819–825.

Silvester, E., Manceau, A., Drits, V.A., 1997. Structure of synthetic monoclinic Na-rich birnessite and hexagonal birnessite.2. Results from chemical studies and EXAFS spectroscopy. Am. Mineral. 82, 962–978.

Sims, J.R., Bingham, F.T., 1968a. Retention of boron by layer silicates, sesquioxides, and soil materials: II. Sesquioxydes. Soil Sci. 32, 364–369.

Sims, J.R., Bingham, F.T., 1968b. Retention of Boron by Layer Silicates, sesquioxides, and soil materials: III. Iron and aluminium-coated layer silicates and soil materials. Soil Sci. 32, 369–373.

Spivack, A.J., Edmond, J.M., 1986. Determination of boron isotope ratios by thermal ionization mass spectrometry of the dicesium metaborate cation. Anal. Chem. 58, 31–35.

Spivack, A.J., Edmond, J.M., 1987. Boron isotope exchange between seawater and the oceanic crust. Geochim. Cosmochim. Acta 51, 1033–1043.

Spivack, A.J., Palmer, M.R., Edmond, J.M., 1987. The sedimentary cycle of the boron isotopes. Geochim. Cosmochim. Acta 51, 1939–1949.

Stumm, W., Morgan, J.J., 1996. Aquatic Chemistry. Wiley, New York.

Su, C., Suarez, D.L., 1995. Coordination of adsorbed boron: a FTIR spectroscopic study. Environ. Sci. Technol. 29, 302–311.

Sverjensky, D.A., 2005. Prediction of surface charge on oxides in salt solutions: revisions for 1:1 (M^+L^-) electrolytes. Geochim. Cosmochim. Acta 69, 225–257.

Szytula, A., Burewicz, A., Dimitrijewic, Z., Krasnicki, S., Rzany, H., Todorovic, J., Wanic, A., Wolski, W., 1968. Neutron diffraction studies of α-FeOOH. Phys. Status Solidi 26, 429–434.

Tossell, J.A., 2006. Boric acid adsorption on humic acids: ab initio calculation of structures, stabilities, ^{11}B NMR and ^{11}B, ^{10}B isotopic fractionations of surface complexes. Geochim. Cosmochim. Acta 70, 5089–5103.

White, A.F., Blum, A.E., Schulz, M.S., Vivit, D.V., Stonestrom, D.A., Larsen, M., Murphy, S.F., Eberl, D., 1998. Chemical weathering in a tropical watershed, Luquillo Mountains, Puerto Rico: I. Long-term versus short-term weathering fluxes. Geochim. Cosmochim. Acta 62, 209–226.

Williams, L.B., Hervig, R.L., Holloway, J.R., Hutcheon, I., 2001a. Boron isotope geochemistry during diagenesis. Part I. Experimental determination of fractionation during illitization of smectite. Geochim. Cosmochim. Acta 65, 1769–1782.

Williams, L.B., Hervig, R.L., Hutcheon, I., 2001b. Boron isotope geochemistry during diagenesis. Part II. Applications to organic-rich sediments. Geochim. Cosmochim. Acta 65, 1783–1794.